

Three-dimensional Graphene-Carbon Nanotubes Composite-Supported PtSn Catalysts with a Tunable Microstructure to Enhance Electrocatalytic Activity for Ethanol Oxidation

Lili Wang¹, Yanting Li¹, Xueli Miao¹, Hao Qin¹, Jiahao Ren¹, Xiaofeng Wang², Zhichun Sun³, Bing Wang^{1,*}

¹ State Key Laboratory of Separation Membranes and Membrane Processes, School of Environment and Chemical Engineering, Tianjin Polytechnic University, 399 Binshui West Road, Tianjin 300387, P. R. China

² State Key Laboratory of Inorganic Synthesis and Preparative Chemistry, College of Chemistry, Jilin University, Changchun 130012, P. R. China

³ Sinosteel Tianjin Geological Research Institute Limited Company, Tianjin 300181, China

*E-mail: bingwang@tjpu.edu.cn

Received: 10 August 2018 / Accepted: 11 September 2018 / Published: 1 October 2018

In this paper, nanostructured platinum-stannum (PtSn) dispersed on a series of composites of graphene oxide (GO) and multi-walled carbon nanotubes (MWNTs), denoted as PtSn/G-CNT have been prepared. Tunable size and distribution of the PtSn nanoparticles was achieved by adjusting the ratio of GO and MWNTs in the composites. The synthesized PtSn/G-CNT, single graphene (PtSn/G) and MWNTs (PtSn/CNT) were applied as anode catalysts for ethanol oxidation. The surface morphology and microstructure of as-prepared catalysts were investigated by scanning electron microscopy, transmission electron microscopy, X-ray photoelectron spectroscopy and X-ray diffraction. The electrocatalytic performance for ethanol oxidation has been estimated by cyclic voltammetry and chronoamperometry in acid media. The PtSn/G-CNT catalysts exhibit higher electrocatalytic activity and stability compared to the PtSn/G and PtSn/CNT. Among all the PtSn/G-CNT catalysts, the optimal PtSn/(2/3G+1/3CNT) catalyst with narrower size, more uniform distribution and higher content of PtSn nanoparticles exhibited higher electrocatalytic activity and stability, which implied the application prospect in the field of ethanol fuel cells.

Keywords: Graphene oxide; Carbon nanotubes; PtSn nanoparticles; Composite support; Electrocatalytic performance

1. INTRODUCTION

Direct ethanol fuel cells (DEFCs), as a promising alternative power source for portable electronic devices, have attracted wide attention due to the high energy density, low pollutant emission,

abundant fuel source and cost cheaper in recent years [1-3]. Metal Pt exhibited high catalytic activity in the catalytic oxidation of ethanol, however, the serious adsorption poison of CO on Pt and the high cost of noble-metal hampered the commercialization of such cells [4]. Generally, it is widely accepted that the Pt catalysts modified by other metals to form Pt-based bimetallic catalysts, such as PtSn [5,6], PtRu [7,8], PtNi [9,10] and PtAu [11,12]. Compare with other bimetallic electrocatalysts, PtSn has shown the best electrocatalytic performance in DEFCs [3].

Moreover, it is great important to explore suitable catalyst support materials which evenly disperse Pt and Pt-based catalyst nanoparticle to obtain better electrochemical performance. The appropriate catalyst support material is not only a convenient route to improve the electrochemical activity of the catalyst, but also decreases the use of noble-metal [7]. In recent years, various structure and morphology carbon-based materials, such as carbon microsphere [13], mesoporous carbon [14], hollow carbon spheres [15], graphene [16] and carbon nanotubes [17] have been extensively investigated for the DEFCs due to their large surface area, high electronic conductivity and low cost. Graphene has been considered as a promising support material for electrocatalysts as its ultrahigh theoretical specific surface area ($2630 \text{ m}^2/\text{g}$), superior electrical conductivity and excellent mechanical properties [18,19]. Usually, the graphene prepared by chemical reduction method is low in cost and can be prepared in batches, however, traditional method led to easy agglomeration of graphene sheets, which greatly reduces the utilization of specific surface area due to the strong van der Waals interactions among the layers of graphene. Therefore, researchers have designed an effective strategy to deal with this challenge: a support body is introduced between the graphene sheets such as carbon nanotubes, metal oxide, or conductive polymer into the interlayer system to prepare graphene composites [19-21]. In this way, the specific surface area and the electrochemical properties of graphene can be significantly improved. Within this field, graphene-carbon nanotubes composites (G-CNT) with three-dimensional (3-D) structure are gradually becoming a research direction. This G-CNT composite material with 3-D structure show more excellent performance than any single material (graphene or carbon nanotubes) such as better isotropic thermal conductivity and 3D microporous network characteristics [22]. Accordingly, G-CNT composite material has a great application prospect in supercapacitor, oxygen reduction reaction, solar cell and fuel cell [23-26]. Several studies have suggested G-CNT was successfully used to the direct methanol fuel cell and showed excellent electrochemical performance [26-28]. The introduction of CNTs can inhibit the aggregation of graphene sheets and construct ion diffusion channels, which ensure rapid diffusion and transport of ions without agglomeration in the preparation process, thus, the particle size and distribution of metal are effectively controlled. Moreover, the formation of G-CNT composite with a 3-D space structure expands the exposure area of the graphene surface and provides much more opportunities for full contact of various ions, thereby promoting the formation of alloys [7, 28]. All above factors have a crucial influence on the electrochemical performance of catalysts. However, G-CNT composite is rarely used in the study of ethanol oxidation. thus, it is significant to study the preparation of G-CNT composite supports metal particle for DEFCs.

In this work, we have presented an effective polyol route for preparation of PtSn/G-CNT catalysts for ethanol electrooxidation. The size and dispersion of the PtSn nanoparticles on catalysts surface were tuned by adjusting the ratio of GO and MWNTs. For comparison, the single graphene and

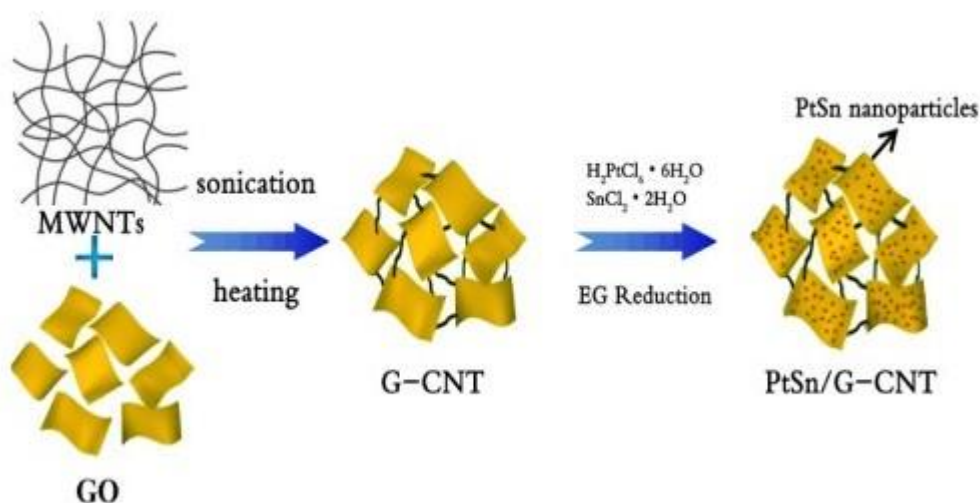
MWNTs supporting PtSn catalysts were also synthesized under the same conditions, denoted as PtSn/G and PtSn/CNT. The morphology and structure of all the synthesized catalysts have been systematically characterized, and their electrocatalytic performance for ethanol electro-oxidation reaction has been examined by cyclic voltammetry and chronoamperometry in acid solution. The present work indicated that the PtSn/G-CNT catalysts exhibit much higher electrocatalytic activity and stability compared to PtSn/G and PtSn/CNT catalysts, and the ratio of GO and MWNTs in catalysts significantly influenced the dispersion, size and the contents of PtSn nanoparticles, which affected the electrocatalytic performance of catalysts. Furthermore, 2:1 (GO:MWNTs), denoted as 2/3G+1/3CNT, appeared to be the best ratio to prepare the G-CNT composite support.

2. MATERIALS AND METHODS

2.1. Materials

$\text{H}_2\text{PtCl}_6 \cdot 6\text{H}_2\text{O}$ (chloroplatinic acid hexahydrate), $\text{SnCl}_2 \cdot 2\text{H}_2\text{O}$ (Tin protochloride dihydrate), Carbon powder, MWNTs (multi-walled carbon nanotubes), EG (ethylene glycol), absolute ethanol, NaOH (Sodium hydroxide), HNO_3 (Nitric acid), H_2SO_4 (Concentrated sulfuric acid, 98wt %) were purchased from Sinopharm Chemical Reagent Co., Ltd. (Tianjin China), MWNTs (multi-walled carbon nanotubes) was purchased from Aldrich, they were all of analytical grade.

2.2. Preparation of catalysts



Scheme 1. Illustration of the preparation process for PtSn/G-CNT catalysts.

GO was prepared by the modified Hummers method in this experiment [29]. Scheme 1 illustrates the prepared procedure of PtSn/G-CNT catalysts. Firstly, the mixture of GO and MWNTs of 60 mg in the required ratio (1:1; 2:1; 3:1), deionized water of 5 mL and EG solution of 80 mL were

mixed and ultra sonicated for 2 h, which were magnetically stirred under flowing nitrogen at 100 °C for 20 h, and then cooled to room temperature. Subsequently, $\text{H}_2\text{PtCl}_6 \cdot 6\text{H}_2\text{O}$ (20 mg mL⁻¹) of 2.7 mL and $\text{SnCl}_2 \cdot 2\text{H}_2\text{O}$ (3.8 mg mL⁻¹) of 2.7 mL were added into the above EG solution to get a composite with 20 wt % metal loading (under the assumption that all Pt and Sn atoms have been reduced by EG). The mixture solution was respectively ultra sonicated and stirred for 1 h, respectively. Thereafter, the pH was adjusted to 11 with saturated solution of NaOH in EG (NaOH-EG) and they were magnetically stirred under flowing nitrogen at 120 °C for 3 h. After cooling, the mixture solution was adjusted to pH < 2 by concentrated HNO_3 , and then stirred for 20 h. The solid was obtained by filtration with PTFE membrane, which was washed with deionized water and ethanol, respectively. Finally, a series of resulting catalysts were obtained after dried at 80 °C for 12 h. The as-prepared samples were denoted as PtSn/(1/2G+1/2CNT), PtSn/(2/3G+1/3CNT) and PtSn/(3/4G+1/4CNT), respectively. For comparison, PtSn/G and PtSn/CNT were also prepared under the same conditions as mentioned above.

2.3 Materials characterization

The morphology of the synthesized samples was investigated with scanning electron microscopy (SEM, Hitachi S-4800). The microstructure and particle size of the catalysts were studied by high-resolution transmission electron microscopy. X-ray diffraction (XRD) measurements were carried out on a Bruker D8 Discover with Cu K α radiation and the diffraction angle ranging from 10° to 90° at a scan rate of 8° min⁻¹. The surface chemical constituents state of the obtained catalysts were analyzed using a X-ray photoelectron spectroscopy (XPS, ESCALAB 250 X-ray photoelectron spectrometer).

2.4 Electrochemical measurements

All electrochemical tests were conducted in a typical three-electrode system using a CHI660D electrochemical workstation (Shanghai Chenhua, China) under N₂ atmosphere at room temperature. A glassy carbon electrode (GCE, 3 mm in diameter) was served as the working electrode, a Pt wire and a saturated calomel electrode (SCE) as the counter and reference electrodes, respectively. The working electrode was prepared as follows: about 5 mg of catalyst powder was dispersed in a mixed solution consisting of 2 mL deionized water and 0.5 mL isopropyl alcohol to form a suspension, which was ultrasonically mixed for 30 min. Then the suspension of 2.5 μL was dropped onto the surface of GCE using a microliter syringe followed by drying at 40 °C. The electrocatalytic active surface area (ECSA) of catalysts was examined by cyclic voltammetry (CV) measurements in 0.5 M H_2SO_4 electrolyte solution at a scan rate of 50 mV s⁻¹, and the ethanol oxidation performance was evaluated using CV tests at a scan rate of 20 mV s⁻¹ in a mixture consisting of 0.5 M H_2SO_4 and 1 M $\text{C}_2\text{H}_5\text{OH}$ with a potential range of -0.2 to 1.0 V. The chronoamperometry (CA) experiments were performed at 0.6 V for 3600 s in the same electrolyte solution to obtain the stability of catalysts.

3. RESULTS AND DISCUSSION

3.1 XRD analysis of the as-prepared materials

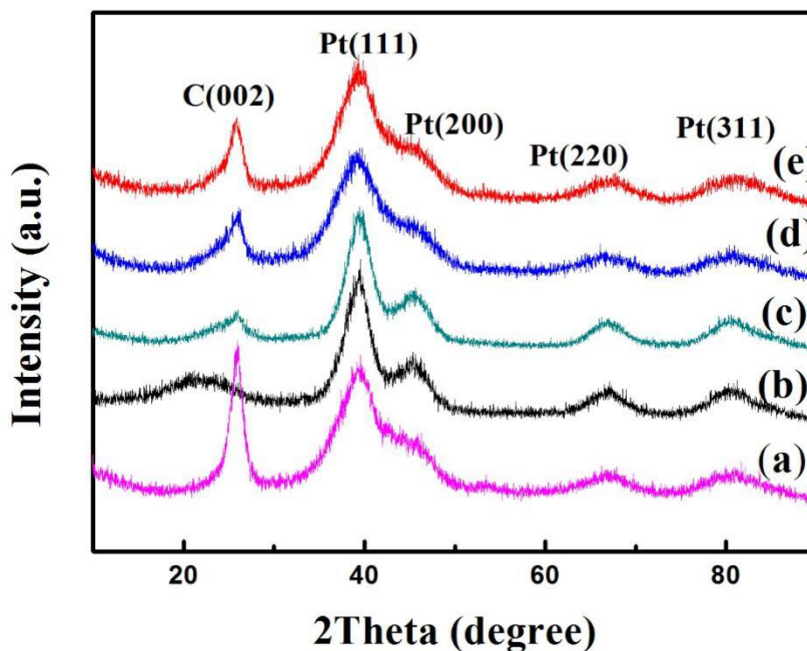


Figure 1. XRD patterns of (a) PtSn/CNT, (b) PtSn/G, (c) PtSn/(3/4G+1/4CNT), (d) PtSn/(2/3G+1/3CNT), and (e) PtSn/(1/2G+1/2CNT).

The XRD patterns of as-prepared PtSn-decorated catalysts were shown in Fig. 1. As illustrated in Fig. 1, the diffraction peak located at around 25° was ascribed to the carbon (002) facet from hexagonal graphite structure. It was noted that graphene and G-CNT revealed a broad (002) peak compared to highly graphitic CNT as a result of unordered stacking and random arrangement of graphene sheets. On the other hand, there are four characteristic peaks of platinum located at around 39° , 46° , 67° , 82° for all samples, which correspond to the (111), (200), (220) and (311) crystal planes of face-centered cubic (fcc) Pt (PDF #65-2868), respectively [30]. Furthermore, the relatively narrow and sharp diffraction peaks of Pt-Sn/G and Pt-Sn/(3/4G+1/4CNT) samples (Fig. 1b-c) displayed a higher crystalline Pt structure compared with Pt-Sn/(2/3G+1/3CNT), Pt-Sn/(1/2G+1/2CNT) and Pt-Sn/CNT samples (Fig. 1d-e and a). Generally, the broad characteristic diffraction peaks of bimetallic catalysts due to the introduction of Sn atoms, which disrupted the arrangement of metallic atoms and interfered with the crystallinity of Pt. The introduction of small Sn atoms shortened the lattice constants of Pt in the fcc structure, accordingly, the broadened diffraction peaks were attributed to the formation of PtSn alloy [31,32]. However, the diffraction peaks of all the bimetallic catalysts in Fig. 1 (a-e) showed the differences resulted from incorporation of CNTs, which built ion diffusion channels as spacers between graphene sheets. Formation of G-CNT with different ratio of GO and MWNTs was conducive to rapid diffusion and transport of ion in the fabrication process, leading to easier formation of PtSn alloys and different alloying degree. In addition, No Sn signal was observed, indicating the Sn

atoms exist in the form of alloys with Pt or amorphous oxide state [31]. The average crystallite size of the as-prepared catalysts can be calculated from Pt (220) diffraction peak according to the Debye–Scherrer formula [33]:

$$D=0.94\lambda_{K\alpha 1}/B_{(2\theta)}\cos\theta_B \quad (1)$$

Where D is the crystallite diameter; $B_{(2\theta)}$ is the full width at half maximum (FWHM) of the diffraction peak; θ_B is the diffraction angle and $\lambda_{K\alpha 1}$ is the incident wave length. The average crystallite sizes of Pt-Sn/G, Pt-Sn/(1/2G+1/2CNT), Pt-Sn/(2/3G+1/3CNT) and Pt-Sn/(3/4G+1/4CNT) samples are 2.4, 2.0, 1.9 and 2.3 nm, respectively.

3.2 SEM and TEM analysis of the as-prepared materials

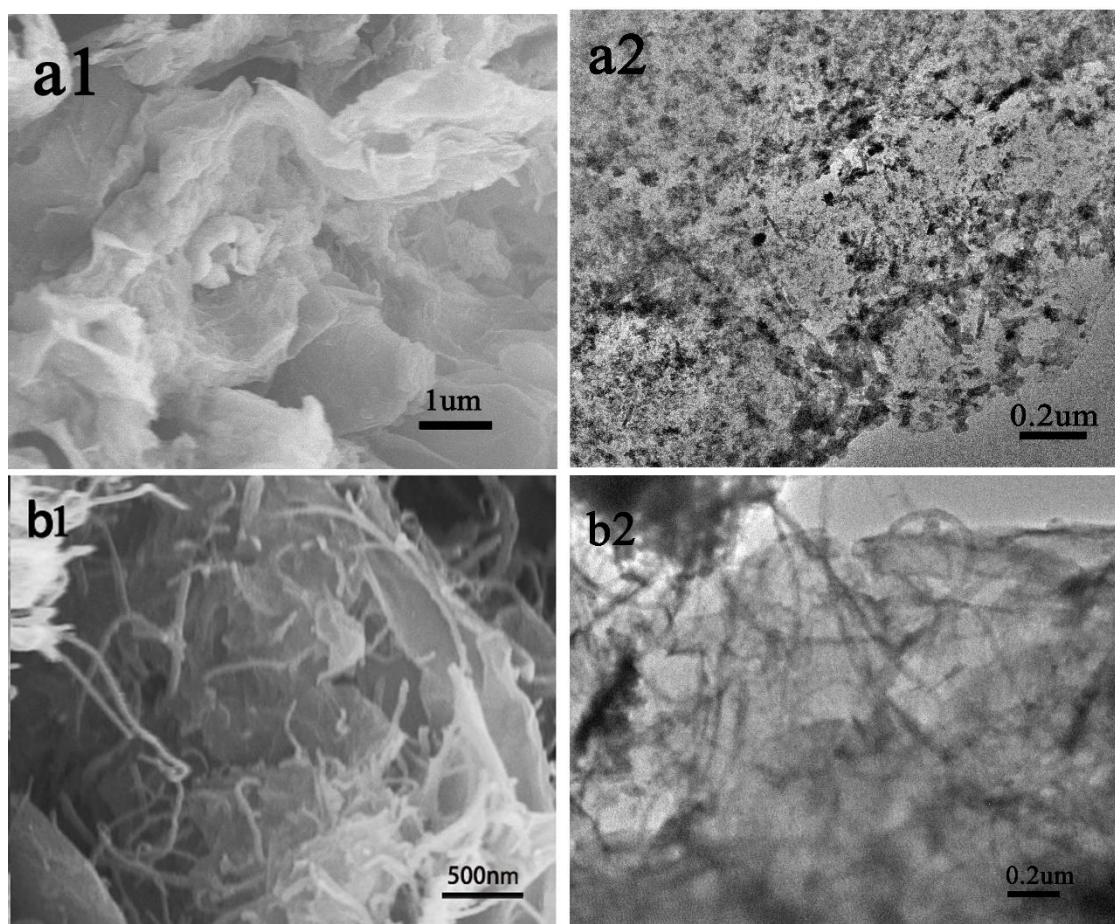


Figure 2. SEM images of (a1) PtSn/G and (b1) PtSn/(2/3G+1/3CNT); TEM images of (a2) PtSn/G and (b2) PtSn/(2/3G+1/3CNT).

The morphologies of the Pt-Sn/G and Pt-Sn/G-CNT catalysts were characterized by SEM and TEM. As illustrated in Fig. 2, the microstructure of Pt-Sn/G and Pt-Sn/(2/3G+1/3CNT) catalysts were quite different. An obvious restacking of graphene sheets of Pt-Sn/G catalyst is shown in Fig. 2 a1-b1. Whereas Pt-Sn/(2/3G+1/3CNT) (Fig. 2 a2-b2) exhibited that CNTs were successfully inserted into the graphene sheets as effective spacers to form a network structure. This formation of three-dimensional structure effectively inhibited the restacking of graphene sheets and enlarged the spaces between

graphene layers, thus, G-CNTs structure might offer a larger exposure surface area in graphene layers, which is beneficial to reduce the agglomeration of metal particles to enhance electrocatalytic performance [7].

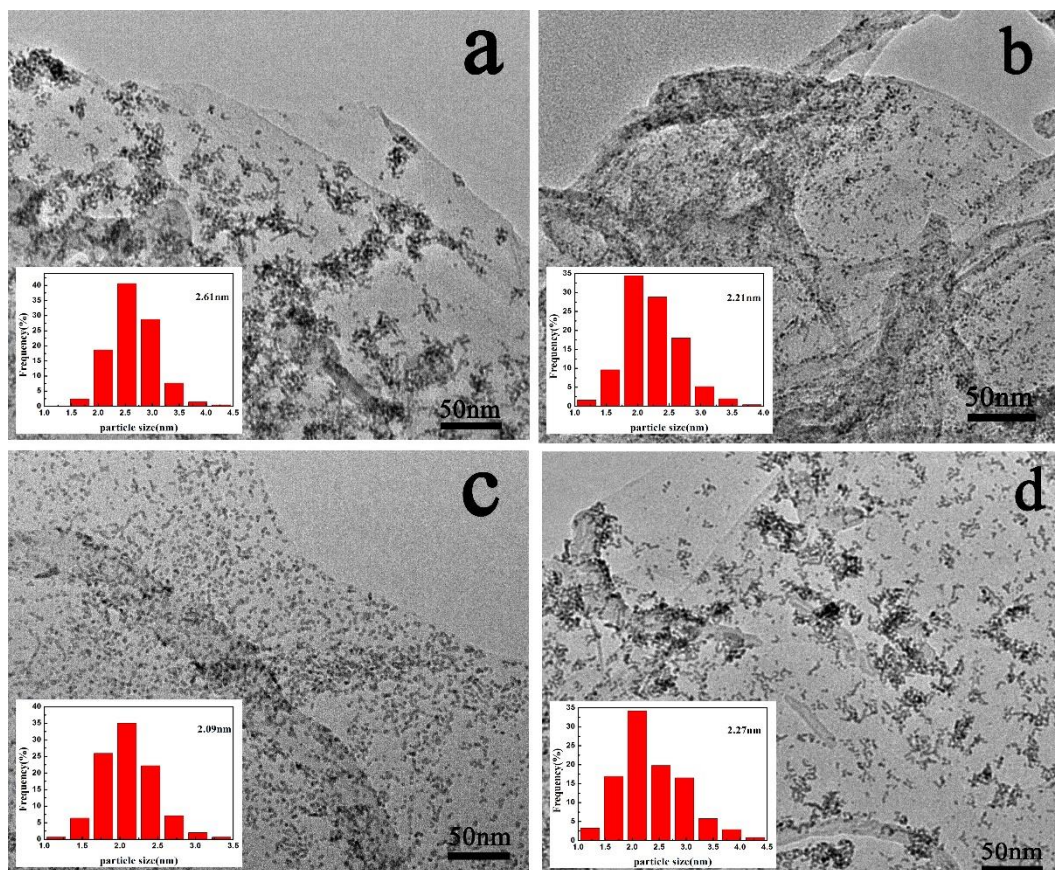


Figure 3. TEM images of (a) PtSn/G, (b) PtSn/(1/2G+1/2CNT), (c) PtSn/(2/3G+1/3CNT) and (d) PtSn/(3/4G+1/4CNT) and the particle size distributions of the metal nanoparticles.

Fig. 3 shows the TEM images and particle size distribution of as-prepared catalysts. It can be found that PtSn nanoparticles have been successfully anchored onto the supports after the chemical reduction. As shown in Fig. 3, the metal particles with sizes ranging from 1 to 5 nm were anchored onto the supports. However, the various distribution of metal nanoparticles in the support were exhibited for PtSn/G, PtSn/(1/2G+1/2CNT), PtSn/(2/3G+1/3CNT) and PtSn/(3/4G+1/4CNT), and the average particle size was 2.61, 2.21, 2.09 and 2.27 nm, respectively. It was visible that the aggregation of metal nanoparticles with graphene alone as a support was fairly serious in Fig. 3a, indicating that the exposed surface area of graphene was too small to primarily disperse the PtSn nanoparticles when the catalyst loading was high. By contrast, after the introduction of CNTs (as illustrated in Fig.3b-d), the size distribution of PtSn/G-CNT catalysts became more uniform and the aggregation of metal nanoparticles was extensively prohibited. It was evident that the catalyst of PtSn/(2/3G+1/3CNT) had the most uniform distribution among all the catalysts. As a support between graphene layer, CNTs played an important role in enlarging exposed surface area of graphene and formatting the ion diffusion channels, which ensured that the metallic ions were rapidly diffused and transported without

agglomeration in the process of catalyst preparation. Hence, 3-D structure of G-CNT effectively controlled the size and distribution of PtSn nanoparticles in catalysts.

3.3 XPS analysis of the as-prepared materials

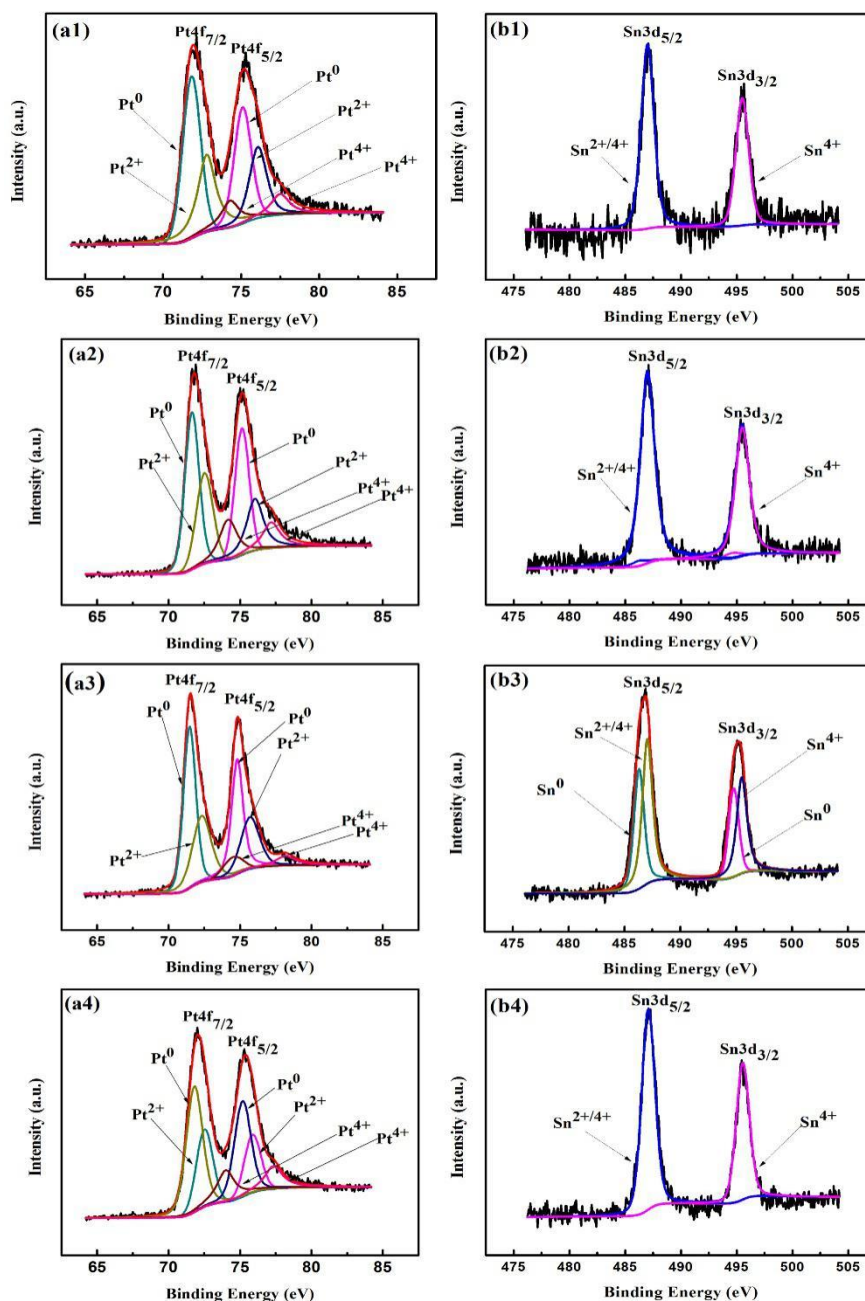


Figure 4. Pt 4f and Sn 3d XPS spectra of the different catalysts: (a1-b1) PtSn/G, (a2-b2) PtSn/(1/2G+1/2CNT), (a3-b3) PtSn/(2/3G+1/3CNT) and (a4-b4) PtSn/(3/4G+1/4CNT).

The electronic structure and elemental compositions of Pt and Sn for the synthesized catalysts was characterized by XPS. The Pt 4f and Sn 3d XPS spectra of Pt-Sn/G and Pt-Sn/G-CNT catalysts are shown in Fig. 4. As shown in Fig. 4 (a1-a4), the Pt 4f spectrum could be fitted into six peaks, and the two most doublets corresponded to Pt 4f_{7/2} and Pt 4f_{5/2} which assigned to metallic Pt⁰ and Pt²⁺

species, respectively [34].

It was visible that two pairs of doublets of Pt⁰4f and Pt²⁺4f accounted for around 80% of the total volume of Pt, indicating that most of the metallic Pt⁴⁺ in platinum acid was reduced to Pt⁰ and Pt²⁺4f. The XPS spectra of Sn 3d are shown in Fig. 4 (b1-b4). The spectrum of the Sn 3d clearly exhibited intense doublets attributed to Sn3d_{5/2} and Sn 3d_{3/2} of the metallic Sn^{2+/4+}, because that the metal Sn was easily oxidized to SnOx at room temperature. However, the Sn 3d XPS spectra of Pt-Sn/(2/3G+1/3CN) sample exhibited two pairs of doublets compared with other samples in Fig. 4b (3). The first peak at 486.3 eV could be attributed to the presence of the oxidation state of Sn⁰, and the other one at 487.1 eV corresponded to oxidation state of Sn^{2+/4+} [35]. This findings indicated that metal Sn was easy to form alloy with metal Pt at nanometer level to enhance its stability in Pt-Sn/(2/3G+1/3CN) catalyst. It was consistent with the results of XRD. The catalyst surface elemental compositions of Pt and Sn were calculated according to the XPS spectra and were listed in Table 1.

Table 1. XPS analysis: elemental atomic concentrations of as-prepared samples.

Catalyst	Pt (at.%)	Sn (at.%)	C (at.%)
PtSn/G	1.73	1	97.27
PtSn/(1/2G+1/2CN)	2.85	1.83	95.32
PtSn/(2/3G+1/3CN)	3.37	2.22	94.41
PtSn/(3/4G+1/4CNT)	2.38	1.41	96.21

This result show that the ratio of GO and MWNTs in G-CNT had significant effects on the elemental compositions of Pt and Sn. As shown in Table 1, the PtSn/G-CNT catalysts show a higher level of metallic components compared with PtSn/G catalyst. The results indicated the higher metallic the higher exposure of the graphene sheet surface area due to the formation of 3-D structure of G-CNT, which facilitated the deposition of metal particles.

3.4 Electrochemical performance of as-prepared materials

To evaluate the potential application of as-prepared catalysts, the electrochemical performance towards the electrooxidation of ethanol in acidic media were investigated.

ECSA has a significant impact which determines the catalytic activity of Pt-based electrocatalysts. To investigate the ECSA of the synthesized catalysts, the CV tests of H₂ adsorption/desorption were performed from -0.2 and 1.0 V (vs. SCE) at the scan rate of 50 mV s⁻¹ in 0.5 M N₂-purged H₂SO₄ aqueous solution at room temperature. The CV curves for the as-prepared catalysts are displayed in Fig. 5, in which typical H₂ adsorption/desorption peaks can be observed between -0.2 V and 0.12 V (vs. SCE) [36]. The ECSA value of different catalysts can be calculated according to Eq.(2) based on the hydrogen adsorption area oxidation peak from Fig. 5 [36]:

$$ECSA = Q_H / (0.21 \times [Pt]) \quad (2)$$

Where Q_H (mC/cm²) represents the amount of charge exchanged during hydrogen desorption

on the Pt surface, $0.21 \text{ (mC/cm}^2\text{)}$ is assumed as the monolayer charge of hydrogen and $[\text{Pt}] \text{ (mg/cm}^2\text{)}$ is the amount loading of Pt on the working electrode.

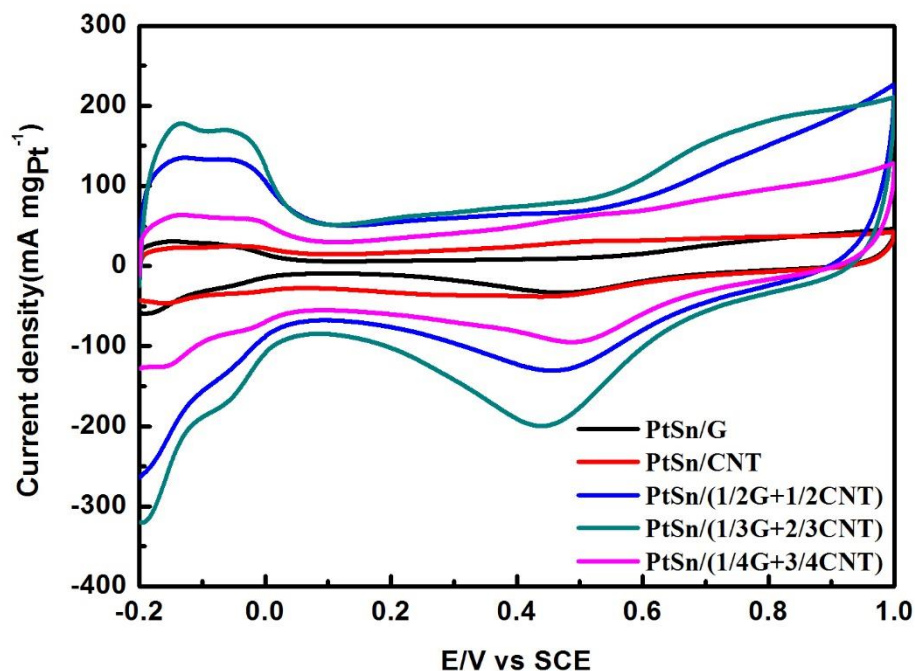


Figure 5. CV curves of H_2 adsorption/desorption on the different catalysts in $0.5 \text{ M H}_2\text{SO}_4$ solution at a scan rate of 50 mV/s .

Table 2. Electrocatalytic activity parameters of the PtSn/G and PtSn/G-CNT catalysts.

Catalyst	ECSA ($\text{m}^2/\text{g}_{\text{Pt}}$)	I_f ($\text{mA}/\text{mg}_{\text{Pt}}$)	I_r ($\text{mA}/\text{mg}_{\text{Pt}}$)	I_f/I_r
PtSn/G	28.77	407.03	370.12	1.10
PtSn/CNT	20.98	259.45	273.87	0.95
PtSn/(1/2G+1/2CNT)	99.43	591.23	643.74	0.92
PtSn/(2/3G+1/3CNT)	226.50	741.52	745.66	1.00
PtSn/(3/4G+1/4CNT)	59.41	512.73	515.56	1.00

The ECSA values of different catalysts are listed in Table 2. As shown in Table 2, the PtSn/(1/2G+1/2CNT), PtSn/(2/3G+1/3CNT) and PtSn/(3/4G+1/4CNT) catalysts displayed the ECSA values of 99.43, 226.50 and 59.41 m^2/g , respectively, which were all higher than the PtSn /G (28.77 m^2/g) and PtSn /CNT (20.98 m^2/g) catalysts, illustrating that G-CNT can be used as a more efficient support compared to alone graphene or CNTs for the ethanol electrocatalytic oxidation. As is well known, Pt content, as the catalytic active substance, is an important factor for the ECSA of catalysts. Hence, it can be concluded that the more Pt active sites were exposed from the interlamination of graphene sheets, and the insertion of CNTs enlarged the space of the supports, which provided more active sites for the electrochemical reaction. Moreover, there was a synergistic effect between Pt and

Sn in PtSn bimetallic catalysts, the increase of Sn content can enhance adsorption/desorption rate of CO oxidation, which will make the deactivated Pt particles obtain catalytic activity once again, thereby also producing more Pt active sites. In addition, the PtSn/(2/3G+1/3CNT) sample had more active sites compared to other G-CNT samples, which may be related to the more uniform distribution of PtSn/(2/3G+1/3CNT) sample, and it contributed to the increase of specific surface area of Pt particles. The loaded Pt nanoparticles could fully contact with the electrolyte, which accelerate charge transfer kinetics of CO oxidative process, and thus improve the electrocatalytic activity [3].

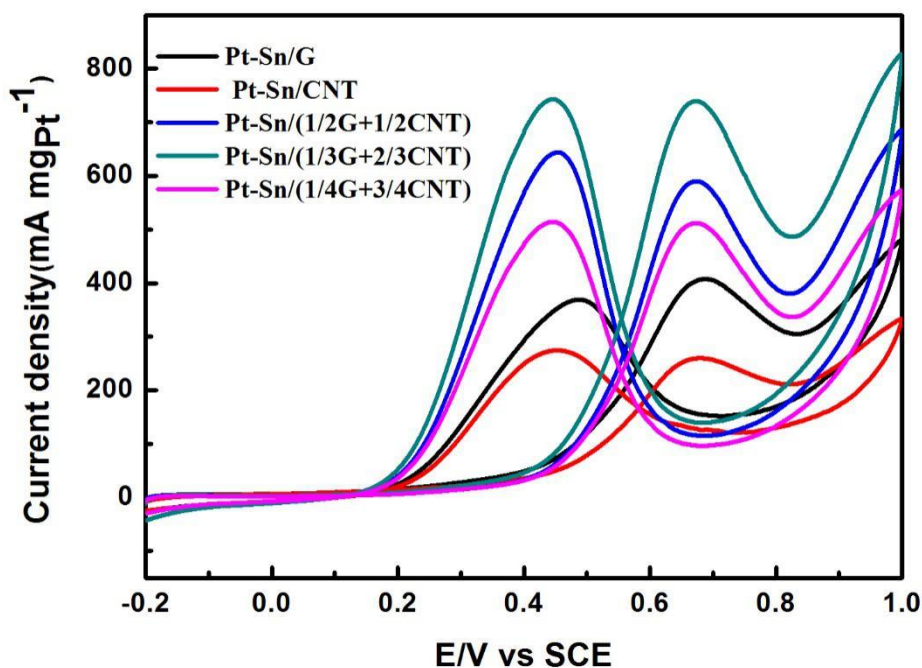


Figure 6. CV curves of Pt-Sn/G and the different Pt-Sn/G-CNT catalysts in 1 M C_2H_5OH + 0.5 M H_2SO_4 solution at a scan rate of 20 mV/s.

The electrocatalytic activities of the different catalysts for ethanol oxidation were measured by CV from -0.2 and 1.0 V (vs. SCE) at 20 mV s^{-1} in a N-purged 1 M C_2H_5OH + 0.5 M H_2SO_4 solution at room temperature. As shown in Fig. 6, all CV curves show two obvious characteristic peaks at forward and backward scans, respectively. The peak at the forward scan (I_f) was the oxidation peak of ethanol, which was attributed to the dehydrogenation of ethanol molecules, and the characteristic oxidation peak (I_r) occurred during backward scans might be assigned to desorption of carbonaceous species during the forward scan. The ratio of the forward peak current density (I_f) to the backward peak current density (I_r) can be used to evaluate the poisoning tolerance of the catalysts [5,36]. A higher I_f/I_r value indicates higher tolerance to intermediate carbon species, suggesting that ethanol can be oxidized to carbon dioxide much more efficiently with less accumulation of intermediate carbonaceous species on the catalyst surfaces [37]. The value of I_f , I_r and I_f/I_r of different catalysts were determined based on Fig. 6 and the data were listed in Table 2. As shown in Table 2, it is evident that the values of I_f for the PtSn/G-CNT catalysts are all higher than that of PtSn/G and PtSn/CNT catalysts, implying that the

PtSn/G-CNT catalysts have higher catalytic activity for ethanol oxidation, which is attributed to the smaller size, narrow distribution and higher load of the PtSn particles of the catalysts. The calculated I_f/I_r values were 1.10, 0.95, 0.92, 1.00, 1.00 for PtSn/G, PtSn/CNT, PtSn/(1/2G+1/2CNT), PtSn/(2/3G+1/3CNT) and PtSn/(3/4G+1/4CNT), respectively. The value of I_f/I_r for PtSn/G-CNT catalysts are slightly lower than PtSn/G. It may be the result of ultrahigh catalytic activity of PtSn/G-CNT catalysts, which accelerates the rate of oxidation of ethanol, leading to the more accumulation of intermediates on the surface of the catalysts. Among of them, PtSn/ (2/3G+1/3CNT) catalyst exhibited highest catalytic activity for ethanol oxidation and good tolerance to carbon containing intermediates, which was due to the optimum size, distribution and loading of the PtSn particles. These results were well consistent with the typical hydrogen adsorption/desorption data of the catalysts, which were measured in 0.5 M H_2SO_4 aqueous solution.

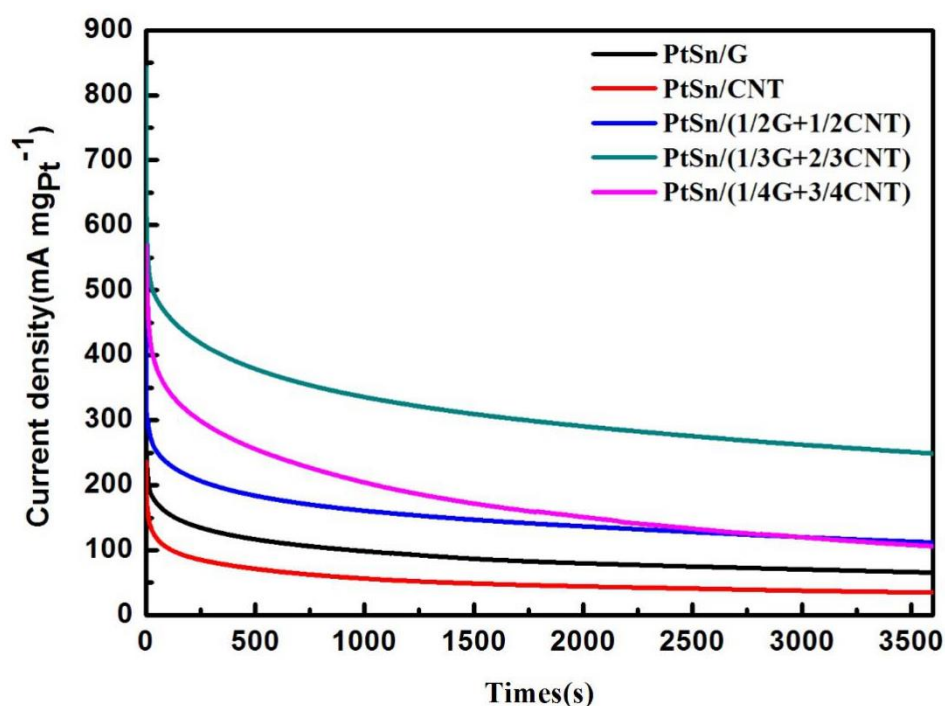


Figure 7. Amperometric *i-t* curves of ethanol oxidation on PtSn/G, PtSn/CNT, and PtSn/G-CNT in 1 M C_2H_5OH + 0.5 M H_2SO_4 solution at 0.6 V (vs. SCE) for 3600 s.

Fig. 7 shows the amperometric *i-t* curves of the different catalysts in 0.5 M H_2SO_4 and 1 M C_2H_5OH solution at a fixed potential of 0.6 V (vs. SCE) for 3600 s at room temperature. As can be seen from the Figure 7, the current densities of all samples showed a similar current decay in the first 50 s. Subsequently, the decay rate slowed down until it became relatively stable. The initial rapid decay of current densities was assigned to the formation of intermediate products such as CO_{ad} adsorbed on the metal nanoparticles surfaces during the ethanol oxidation reaction, resulting in deactivation of active site of catalyst [38,39]. The order of current densities at 3600 s for different catalysts are as follows: PtSn/(2/3G+1/3CNT) > PtSn/(1/2G+1/2CNT) > PtSn/(3/4G+1/4CNT) > PtSn/G > PtSn/CNT. The current densities of PtSn/G-CNT catalysts are obviously higher than PtSn/G and PtSn/CNT catalyst, indicating that the introduction of CNT between graphene sheets can enhance

the catalytic activity by building ion transport channel and enlarging specific surface area of catalysts. Besides, PtSn/(2/3G+1/3CNT) showed the lowest current decay after test for 500 s, suggesting an increased stability for ethanol oxidation. This finding was consistent with the CV results. Hence, the high catalytic activity and stability for PtSn/(2/3G+1/3CNT) were attributed to the more perfect 3-D space structure due to appropriate quantity of CNT.

Table 3. Comparison of the activities for ethanol oxidation of PtSn/(2/3G+1/3CNT) and catalysts reported in literatures.

Catalyst	Pt (wt.%)	ESCA ($\text{m}^2/\text{g}_{\text{Pt}}$)	The peak current density ($\text{mA}/\text{mg}_{\text{Pt}}$)	literature
PtSn/G-A	18.5	42.2	548.9	[1]
PtSn/NG-600	0.64	71	590	[3]
PtRu/GS-CNTs	20	118.69	192	[7]
Pt/HCSs	20	142	138	[15]
Pt/T-fGN	20	39.42	180	[16]
PtSn/HCH-N0.5	20	102	430	[40]
PtSn/(2/3G+1/3CNT)	20	226.5	741.52	This work

In addition, other types of catalysts reported in literatures were compared to PtSn/(2/3G+1/3CNT). As shown in Table 3, the PtSn/(2/3G+1/3CNT) has the largest ESCA value and the peak current density is relatively high. This proved that the catalyst prepared with the carrier of 3-D structure of graphene and carbon nanotube can greatly increase the active area of the catalyst and significantly increase the current density.

4. CONCLUSIONS

In conclusion, this study documented a new method which successfully enhanced both the utilization of graphene sheet and the electrochemical activity of PtSn catalysts. This enhancement was achieved by introducing short MWCNTs to build ion transport channel and enlarge the spaces among graphene sheets. It was found that the PtSn/G-CNT catalysts possessed a relatively more uniform distribution, smaller particle size of PtSn nanoparticle and a higher PtSn alloy content compared with PtSn/G and PtSn/CNT catalysts, which were due to the formation of 3-D structure of the G-CNT composite material. Therefore, the considerably higher value of ECSA, I_p/I_r and a larger current density for ethanol oxidation were obtained. The results showed the dispersion, size and contents of PtSn nanoparticles were controlled by adjusting the ratio of GO and MWNTs, which influenced the catalytic activity of ethanol oxidation. The optimal Pt-Sn/(2/3G+1/3CNT) catalyst with narrower size and more uniform had higher electrocatalytic activity and stability compared to other PtSn/G and PtSn/CNT for the ethanol oxidation, which indicated the prospect for DEFCs applications.

ACKNOWLEDGMENTS

This research was supported by the State Key Laboratory of Inorganic Synthesis and Preparative Chemistry of Jilin University (No. 2017-31).

References

1. Y. Wang, X. Wang, Y. Wang, J. Li, *Int. J. Hydrogen Energy*, 40 (2015) 990-997.
2. L.C. Ordóñez, B. Escobar, R. Barbosa, Y. Verde-Gómez, *J. Appl. Electrochem.*, 45 (2015) 1205-1210.
3. J. Yu, M. Jia, T. Dai, F. Qin, Y. Zhao, *J. Solid State Electrochem.*, 21 (2016) 967-974.
4. G.R. Salazar-Banda, K.I.B. Eguiluz, M.M.S. Pupo, H.B. Suffredini, M.L. Calegaro, L.A. Avaca, *J. Electroanal. Chem.*, 668 (2012) 13-25.
5. A. Amorim, L. Parreira, J. Silva, M. dos Santos, *J. Brazil. Chem. Soc.*, 28 (2016) 1091-1097.
6. L. Pastor-Pérez, A. Sepúlveda-Escribano, *Fuel*, 194 (2017) 222-228.
7. Y.-S. Wang, S.-Y. Yang, S.-M. Li, H.-W. Tien, S.-T. Hsiao, W.-H. Liao, C.-H. Liu, K.-H. Chang, C.-C.M. Ma, C.-C. Hu, *Electrochim. Acta*, 87 (2013) 261-269.
8. Z. Yang, S. Xu, J. Xie, J. Liu, J. Tian, P. Wang, Z. Zou, *J. Appl. Electrochem.*, 46 (2016) 895-900.
9. Y.-Y. Zhou, C.-H. Liu, J. Liu, X.-L. Cai, Y. Lu, H. Zhang, X.-H. Sun, S.-D. Wang, *Nano-Micro Lett.*, 8 (2016) 371-380.
10. Q. Wang, G. Wang, H. Tao, Z. Li, L. Han, *RSC Adv.*, 7 (2017) 8453-8459.
11. C. Du, X. Gao, Z. Zhuang, C. Cheng, F. Zheng, X. Li, W. Chen, *Electrochim. Acta*, 238 (2017) 263-268.
12. P. Song, L.-P. Mei, A.-J. Wang, K.-M. Fang, J.-J. Feng, *Int. J. Hydrogen Energy*, 41 (2016) 1645-1653.
13. J. Zhang, J. Zhou, D. Wang, L. Hou, F. Gao, *Electrochim. Acta*, 191 (2016) 933-939.
14. M.A. Hoque, D.C. Higgins, F.M. Hassan, J.-Y. Choi, M.D. Pritzker, Z. Chen, *Electrochim. Acta*, 121 (2014) 421-427.
15. X. Bo, J. Bai, J. Ju, L. Guo, *J. Power Sources*, 196 (2011) 8360-8365.
16. Y. Li, L. Han, B. An, Y. Wang, L. Wang, X. Yin, J. Lu, *J. Mater. Sci. - Mater. Electron.*, 27 (2016) 6208-6215.
17. J. Wang, R. Huang, Y. Zhang, J. Diao, J. Zhang, H. Liu, D. Su, *Carbon*, 111 (2017) 519-528.
18. L. Jiang, Z. Fan, *Nanoscale*, 6 (2014) 1922-1945.
19. B.F. Machado, A. Marchionni, R.R. Bacsá, M. Bellini, J. Beausoleil, W. Oberhauser, F. Vizza, P. Serp, *J. Energy Chem.*, 22 (2013) 296-304.
20. R. Kannan, A.R. Kim, J.S. Kim, D.J. Yoo, *Int. J. Hydrogen Energy*, 41 (2016) 18033-18043.
21. J. Zhong, G.-X. Zhou, P.-G. He, Z.-H. Yang, D.-C. Jia, *Carbon*, 117 (2017) 421-426.
22. D. Zhao, Z. Li, L. Liu, Y. Zhang, D. Ren, J. Li, *Acta Chim. Sinica.*, 72 (2014) 185.
23. Q. Yang, S.-K. Pang, K.-C. Yung, *J. Power Sources*, 311 (2016) 144-152.
24. J. Zhao, Y. Liu, X. Quan, S. Chen, H. Zhao, H. Yu, *Electrochim. Acta*, 204 (2016) 169-175.
25. J. Zhang, M. Yu, S. Li, Y. Meng, X. Wu, J. Liu, *J. Power Sources*, 334 (2016) 44-51.
26. F. Ye, X. Cao, L. Yu, S. Chen, W. Lin, *Int. J. Electrochem. Sci.*, 7 (2012) 1251-1265.
27. T. Yuan, J. Yang, Y. Wang, H. Ding, X. Li, L. Liu, H. Yang, *Electrochim. Acta*, 147 (2014) 265-270.
28. N. Jha, R.I. Jafri, N. Rajalakshmi, S. Ramaprabhu, *Int. J. Hydrogen Energy*, 36 (2011) 7284-7290.
29. W.S. Hummers, R.E. Offeman, *J Am Chem Soc* 80:1339, *J. Amer. Chem. Soc.*, 80 (1958).
30. H.Y. Zhu, C.D. Gu, X. Ge, J.P. Tu, *Electrochim. Acta*, 222 (2016) 938-945.
31. H. Song, M. Luo, X. Qiu, G. Cao, *Electrochim. Acta*, 213 (2016) 578-586.
32. R. Crisafulli, R.M. Antoniassi, A. Oliveira Neto, E.V. Spinacé, *Int. J. Hydrogen Energy*, 39 (2014) 5671-5677.
33. Y. Ma, H. Wang, S. Ji, V. Linkov, R. Wang, *J. Power Sources*, 247 (2014) 142-150.

34. Y. Xin, J.-g. Liu, Y. Zhou, W. Liu, J. Gao, Y. Xie, Y. Yin, Z. Zou, *J. Power Sources*, 196 (2011) 1012-1018.
35. P. Bommersbach, M. Chaker, M. Mohamedi, D. Guay, *J. Phys. Chem. C*, 112 (2008) 14672-14681.
36. Y. Li, W. Gao, L. Ci, C. Wang, P.M. Ajayan, *Carbon*, 48 (2010) 1124-1130.
37. Y. Hao, Y. Yang, L. Hong, J. Yuan, L. Niu, Y. Gui, *ACS Appl. Mat. Interfaces*, 6 (2014) 21986-21994.
38. J. Tayal, B. Rawat, S. Basu, *Int. J. Hydrogen Energy*, 36 (2011) 14884-14897.
39. H. Wang, Q. Zhao, Q. Ma, *Ionics*, 21 (2014) 1703-1709.
40. X. Wu, H. Qin, Y. Li, L. W, Y. Shen, J. Tang, X. Wang, J. Ren, B. Wang, *Int. J. Electrochem. Sci.*, 13 (2018) 3091-3106.

© 2018 The Authors. Published by ESG (www.electrochemsci.org). This article is an open access article distributed under the terms and conditions of the Creative Commons Attribution license (<http://creativecommons.org/licenses/by/4.0/>).